Applied Catalysis B: Environment and Energy 398 (2026) 127017

Contents lists available at ScienceDirect

Applied Catalysis B: Environment and Energy

journal homepage: www.elsevier.com/locate/apcatb

How electrolyte properties and applied potential impact pathways and performance in electrochemical nitrate reduction

Ana Daniela Azúa-Humara [a,b], Christina Oeß [a], Anna K. Mechler [c,d,e], Hermann Tempel [a], Rüdiger-A. Eichel [a,b,f], Ana Laura Luna [a,*]

[a] Institute of Energy Technologies, Fundamental Electrochemistry (IET-1), Forschungszentrum Jülich GmbH, Jülich 52425, Germany
[b] Institute of Physical Chemistry, RWTH Aachen University, Aachen 52074, Germany
[c] Institute of Energy Technologies, Electrochemical Process Engineering (IET-4), Forschungszentrum Jülich GmbH, Jülich 52425, Germany
[d] Electrochemical Reaction Engineering (AVT.ERT), RWTH Aachen University, 52074, Germany
[e] JARA-ENERGY, Jülich 52425, Germany
[f] Faculty of Mechanical Engineering, RWTH Aachen University, 52062, Germany

ARTICLE INFO

Keywords:
Nitrate reduction
Electrocatalysis
Ammonia
Electrolyte effect
Cation effect

ABSTRACT

Electrochemical nitrate reduction reaction (NO_3RR) is a promising route for the valorization of nitrate pollutants into ammonia; however, while extensive efforts have focused on catalyst development, the influence of electrolyte properties on NO_3RR performance has been largely overlooked and remains poorly understood. Here, we show that the electrolyte alone contributes significantly and systematically to the reaction, independent of catalyst identity. To identify the electrocatalytic trends driven by the electrolyte, key parameters —including pH, nitrate concentration, and co-existing cations— were investigated through rationally designed electrochemical experiments performed across multiple metals (Cu, Ag, Pd, Au, Bi, Mo, and Ti), enabling differentiation of catalyst-specific behavior from electrolyte-driven effects. We find that pH and co-existing cations are critical, as they modulate interfacial proton availability, nitrate adsorption, intermediate stabilization, and controlled protonation toward ammonia formation. The effect of nitrate concentration depends on these two parameters as well as the applied potential. Importantly, our study highlights a commonly neglected aspect: alkali metal cations are not simple spectators but act as critical electrostatic field mediators in NO_3RR. This work provides guidance for engineering electrolytes for nitrate-to-ammonia electrocatalytic systems and calls for redefining alkali metal cations as a key tuning parameter.

1. Introduction

Nitrate pollutants in water pose critical risks to both the environment and human health [1–4]. The primary source of nitrate pollution is the intensive use of nitrogen-based fertilizers in agriculture [5], where nearly half of the globally applied nitrogen (~150 million tons per year) is lost and contaminates natural water systems as nitrate [1,4]. This leads to problems such as eutrophication and contamination of drinking water. Elevated nitrate levels in drinking water are associated with serious health issues, including methemoglobinemia, gastric cancer, and birth defects [2]. Although the World Health Organization (WHO) recommends a maximum nitrate concentration of 50 mg L^{-1} in drinking water [4,6], concentrations in regions with intensive crop production can exceed this threshold by up to 700% [1].

In addition to agriculture, industrial activities such as pharmaceutical production, chemical synthesis, explosive manufacturing, and metal finishing significantly contribute to nitrate pollution [7–9]. Their effluents can contain several thousand mg L^{-1} of nitrates; for example, metal-finishing effluents reach ~3100 mg L^{-1}, while explosive manufacturing can be up to 10-fold higher [7,8]. Industrial effluents must be treated before discharge to prevent environmental contamination.

Electrochemical nitrate reduction towards ammonia offers a promising solution to simultaneously mitigate nitrate pollution and produce valuable ammonia [10–13], a high-demand chemical with a global production of ~175 million tons and a market value of US$67 billion [14]. Although unlikely to meet the entire global ammonia demand, NO_3RR holds significant potential to mitigate nitrate pollution, reduce

* Corresponding author.
E-mail address: a.luna.barron@fz-juelich.de (A.L. Luna).

https://doi.org/10.1016/j.apcatb.2026.127017
Received 5 March 2026; Received in revised form 30 April 2026; Accepted 24 May 2026
Available online 25 May 2026

the need for virgin N-fertilizer production, and advance a sustainable, circular nitrogen economy.

Due to low nitrate concentrations (particularly in groundwater), low ionic conductivity, and complex and variable background matrices, electrochemical nitrate reduction requires a pre-separation step. Advanced technologies such as reverse osmosis or electrocapacitive removal can be employed for this initial separation in a stepwise process [15–17]. Alternatively, integrated separation–reaction systems have also been proposed [18]. Although these approaches differ in configuration, both aim to produce nitrate-enriched streams that are subsequently converted into ammonia. Under such conditions, the overall performance of NO_3RR depends critically on the interplay between catalyst activity, electrolyte properties, and the applied reaction conditions.

NO_3RR research has largely focused on developing electrocatalysts (e.g., metals, alloys, oxides, sulfides, oxysulfides, and phosphides [19–25]) that achieve high current densities at low overpotentials and high ammonia selectivity, despite the similar thermodynamic potentials of the possible products [13,26]. In contrast, the role of electrolyte properties —such as pH, nitrate concentration, and the identity of co-existing ions— has received comparatively limited and unsystematic attention. This limited understanding of electrolyte effects is nontrivial, as the electrolyte defines the boundary conditions governing all processes at the electrode–electrolyte interface, thereby directly influencing catalyst activity and ultimately the performance of NO_3RR systems.

Although pH has been shown to influence NO_3RR, significant inconsistencies remain regarding which pH conditions favor ammonia formation and the underlying mechanisms this effect. For example, Jaramillo et al. observed higher ammonia selectivity at pH 0.77 than at pH 13 over a potential range of −0.75 to −1.25 V vs RHE and concluded that high proton concentration promotes ammonia selectivity in NO_3RR [17]. Conversely, Gou and coworkers [27] reported a different pH-dependent trend in their study using Cu foil as a model electrode, finding that ammonia formation is favored at pH 13. They attributed this behavior to more efficient NH_3 desorption in alkaline electrolytes compared with acidic ones. Luo et al. observed higher NH_3 yield rates and faradic efficiencies on Cu_2O nanocubes in acid electrolytes, within a potential window of −0.4 to −0.8 V vs RHE, compared to neutral and alkaline electrolytes [28].

In nitrate concentration studies, most reports show an increase in nitrate reduction activity with increasing nitrate concentration in the electrolyte [17,29]. This behavior is commonly attributed to the greater availability of nitrates at the electrode interface, which enhances their probability of reduction. However, several experimental and theoretical studies have shown that NO_3^- binds only weakly to metal surfaces and gradually desorbs as more negative potentials are applied due to their negative charge [30–33]. Based on these findings, it is evident that the conventional explanation of the concentration effect does not fully account for its impact on NO_3RR activity. More importantly, this indicates that the phenomena governing concentration-dependent behavior in NO_3RR remain poorly understood and call for further investigation.

Co-existing alkali cations (Li^+, Na^+, K^+, and Cs^+) are widely recognized to influence the activity of electrocatalytic reactions such as hydrogen evolution and CO_2 reduction [34–38]. In contrast, their effect in NO_3RR has been largely overlooked, and they are often treated as inert spectators. However, emerging studies suggest that these cations can influence NO_3RR performance [39], indicating that their impact may be more complex than generally assumed. This raises the question of whether co-existing cations are truly passive species or actively participate in the NO_3RR, and, if so, how, and under which reaction conditions their effects become significant.

All the above observations highlight that electrolyte properties influence NO_3RR performance through interrelated phenomena that remain incompletely understood. Therefore, systematic studies of electrolyte effects across different metal surfaces are required to gain insights into the contributions of individual electrolyte properties and their interplay in the key steps of nitrate reduction. This understanding is key to advancing NO_3RR performance.

Here, we systematically investigate how and to what extent electrolyte properties and applied potential influence NO_3RR to NH_3. To this end, we design electrochemical evaluations that isolate the effects of pH, nitrate concentration, and coexisting cations on the selectivity and activity towards NH_3. We apply this framework to Cu, Ag, Pd, Au, Bi, Mo, and Ti electrodes, enabling us to disentangle intrinsic, catalyst-specific behavior from effects arising solely from the electrolyte. Furthermore, we assess whether the impact of such electrolyte properties depends on the applied potential. In addition to NH_3, we quantify nitrogen-containing by-products as well as competing H_2 formation to elucidate the mechanistic changes induced by electrolyte composition and potential. We show that alkaline electrolytes (pH 13) benefit ammonia formation rates for all the metals, independent of intrinsic relative activity. Our findings reveal that the electrolyte pH steers the reaction pathway in a consistent fashion, independently of the metal. While such pH-electrolyte effects remain largely invariant with applied potentials, ammonia selectivity is sensitive to them. We further demonstrate that cations, often overlooked in NO_3RR studies, play a critical role in mediating the interfacial electrostatic field, enabling NO_3^- ions to overcome their natural repulsion from the polarized electrode and reach the surface for conversion.

2. Methods

Materials and Reagents were obtained from commercial suppliers and used without further purification. Electrochemical-grade Ag, Pd, and Ti foils were purchased from Redox.Me. Bi (99.999%), Mo (99.9%), Au, and Cu foils were obtained from GoodFellow. Oxalic acid (99.999%), cesium nitrate (99.99%), cesium hydroxide monohydrate (≥99.5%), boric acid (≥99.5%), potassium nitrate (≥99.0%), Bis-(2-hydroxyethyl)iminotris(hydroxymethyl)methane (BIS-TRIS, ≥99.0%), *p*-hydroxybenzoic acid (99.0%), potassium nitrite (≥97.0%), and potassium hydroxide (≥85.0%) were purchased from Sigma-Aldrich. Nitric acid (65%) and ammonium chloride (analytical grade) were obtained from Merck. Hexacyanoferrate (III) (≥99.0%) was purchased from ACS. 10-crown-6 (99%) was obtained from Thermo Scientific. Argon and helium (BIP 6.0, 99.9999%), as well as hydrogen, nitrous oxide, and nitrogen gases, were supplied by Air Products. Ultrapure deionized water with a resistivity > 18 MΩ cm, measured at room temperature.

2.1. Electrochemical experiments

Electrochemical measurements were conducted in a gas-tight electrochemical cell (2-CMEC, Redox) with two compartments separated by a porous ceramic frit. The cell was operated in a three-electrode configuration, consisting of a metal foil electrode, a platinum wire counter electrode, and a commercial Ag/AgCl (3 M KCl, Redox) reference electrode. Polycrystalline metal foils (Ag, Au, Bi, Pd, Mo, Ti, and Cu) with an exposed area of $4 \times 4\ mm^2$ were used as working electrodes. Prior to each experiment, the foils were mechanically polished with sandpaper and thoroughly rinsed with ultrapure deionized water to ensure a clean surface.

All measurements were performed using a Bio-Logic SP-300 potentiostat, with applied potentials referenced to the reversible hydrogen electrode (RHE), calculated using Eq. 1 and the manufacturer-specified standard potential of the Ag/AgCl reference electrode (0.207 V vs SHE). IR-drop compensation of 80% was applied during all electrochemical measurements. The compensation was based on the measured electrolyte resistance, which ranged from 8 and 24 Ω depending on the salt concentration, determined by high-frequency impedance testing. The electrochemical cells were filled with 30 mL of the selected electrolyte, which was saturated with argon by bubbling at a flow rate of 100 mL min^{-1} for 10 min. The cell was then sealed and magnetically stirred at 300 rpm using a cylindrical PTFE stirring bar (30 mm length)

to ensure efficient mass transport to and from the cathode, as verified by pre-hydrodynamic tests (**SI-1**). Before initiating electrochemical measurements, the open-circuit potential was recorded for 5 min to ensure system stability. Subsequently, a potential was applied according to the specific experiment for 1 h. All experiments were carried out at room temperature under ambient conditions. Detailed conditions for each experimental set are described below.

$$E_{RHE} = E_{Ag/AgCl} + 0.207 + 0.059 \quad pH \tag{1}$$

Effect of Electrolyte pH on NO_3RR. To identify pH-dependent trends, electrochemical measurements were conducted on all seven electrodes in 0.3 M NO_3^- electrolyte solutions at pH 1 and 13, adjusted using HNO_3 and KOH, respectively. Detailed electrolyte preparation is provided in the Supplementary Information (**SI-2**). A constant potential of −0.75 V vs RHE was applied.

Interplay between Applied Potential and Electrolyte pH. To evaluate how comparable driving forces influence the identified pH-dependent trends, electrochemical measurements were performed at applied potentials of −0.25, −0.50, −0.75, and −1.00 V vs RHE. Experiments were conducted on Pd, Ti, and Cu electrodes in 0.3 M NO_3^- electrolytes at pH 1 and 13.

Heatmaps of Initial Nitrate Concentration vs Applied Potential. In these experiments, electrolytes with nitrate concentrations of 0.1, 0.3, and 0.5 M were used at pH 1 and pH 13. The applied potentials were −0.25, −0.50, −0.75, and −1.00 V vs RHE. Pd, Ti, and Cu were used as electrodes.

Influence of Co-existing Cations. The activity toward ammonia formation with two different cations was evaluated at nitrate concentrations of 0.1, 0.3, and 0.5 M, at pH 1 and pH 13. To prepare the electrolytes, cesium and potassium salts were used, as described in the Supplementary Information (**SI-2**). A constant potential of −0.75 V vs RHE was applied.

Each electrochemical measurement was performed at least three times to assess reproducibility. Arithmetic means of replicate measurements are reported, with standard deviations shown as error bars. For Faradaic efficiencies, data are presented as stacked bars to visualize the mean product distribution. Because product Faradaic efficiencies are compositional quantities with correlated uncertainties, the standard deviation is reported only for the total Faradaic efficiency. The statistical analysis methodology is described in detail in Supplementary Information (**SI-3**).

2.2. Product quantification

Liquid and gas samples were collected from the electrochemical cell after each experiment to identify and quantify the generated products. Ammonia exists in different forms depending on the reaction pH: at pH 1 as NH_4^+ and at pH 13 as NH_3. Ammonia was quantified by ion chromatography (IC, Shimadzu) in the form of NH_4^+ after adjusting the sample pH to approximately 3 to shift the equilibrium towards NH_4^+ in all systems (see details in **SI-4**). Under alkaline conditions, no NH_3 was lost from the electrolyte, as the NH_3 concentrations produced in our experiments where low (< 300 ppm), as shown in **SI-5.** Therefore, NH_4^+ quantified after pH adjustment corresponds to the NH_3 initially formed. The IC analysis was performed using a Shim-pack IC-C4 column (7 μm; 150 ×4.6) with a conductivity detector.

The concentration of NO_2^- was determined by non-suppressor anion chromatography (Shimadzu) equipped with a Shim-pack IC-A3 column (5 μm, 150 ×4.6) and a conductivity detector. Gas products (i.e., N_2O, N_2, and H_2) were quantified using gas chromatography (GC-2030N, Shimadzu).

Gas separation was achieved using Molsieve 5 A (0.32 mm ID, 30 μm df, 50 m) and Paraplot Q (0.32 mm ID, 10 μm df, 50 m) columns. Detection was performed with a dielectric-barrier discharge ionization detector (BID-2030). A detailed description of the gas and liquid sample handling procedures is provided in **SI-4**.

2.3. Electrode characterization

X-ray diffraction (XRD) patterns were recorded ex situ using a Panalytical Empyrean diffractometer with Molybdenum Kα radiation and β filter on the diffracted beam side. The generator was operated at 50 kV and 40 mA. The angular range $5 \leq 2\theta \leq 55^\circ$ was scanned stepwise/continuously with step time of 59.69 s. Measurements were performed in transmission mode, with the samples sandwiched between two Kapton foils.

For XRD measurements, the electrodes were removed after electrochemical measurements, thoroughly rinsed with deionized water to remove residual electrolyte, dried under an Ar flow (10 mL min^{-1}) at room temperature, and subsequently analyzed by XRD.

Crystalline phase identification was done by comparing the obtained patterns with those reported in the Inorganic Crystal Structure Database (ICSD) [40] and Crystallography Open Database (COD) [41].

3. Results and discussion

3.1. Effect of electrolyte pH on NO_3RR

To assess the influence of electrolyte pH on NO_3RR, we evaluated the catalytic performance of seven metal electrodes at a fixed potential of –0.75 V vs RHE in 0.3 M NO_3^- electrolyte at pH 1 and 13. These pH values were chosen to represent extreme acidic and alkaline regimes, maximizing the contrast in proton availability and enabling clear identification of pH-dependent effects. Additionally, these extreme pH conditions ensure well-defined and stable reaction environments that cannot be achieved at intermediate pH values (e.g., 3, 5, 9, and 11), as detailed in **SI-2**. The metals were selected to span a broad range of intrinsic chemical properties and surface chemistries, enabling identification of pH-dependent trends in NO_3RR activity and selectivity across chemically diverse electrocatalysts and isolating behaviors that persist despite differences in intrinsic catalyst properties and that can therefore be attributed to pH effects. The applied potential of –0.75 V vs RHE was chosen based on CV measurements (Figure S1), which confirmed that all metals were catalytically active at this potential and excluded mass-transport limitations under the applied conditions. Total and partial current densities (j_{total} and j_i), proportional to formation rates, were used as descriptors of catalytic activity, whereas Faradaic efficiencies (FE_i) were used to quantify selectivity.

The results show that metal activity was strongly influenced by electrolyte pH, with higher total current densities (j_{total}) observed at pH 13 than at pH 1 (Fig. 1**a**). All the metals exhibited an increase in their partial current density to ammonia (j_{NH_3}) when the reactions were carried out at pH 13 (Fig. 1**b**), suggesting that NH_3 formation proceeds more efficiently in electrolytes with limited proton availability. These results highlight that although protons are required for the reduction of nitrate to ammonia, an excess proton concentration (as in pH 1) does not necessarily enhance NH_3 rate formation and may even be detrimental.

To elucidate the origin of this pH dependence, we analyzed the by-product formation rates alongside the competing hydrogen evolution reaction (HER). We first focus on HER. As shown in Fig. 1**c**, all investigated metals exhibited higher partial current densities for HER at pH 1 than at pH 13, with increases ranging from ∼20–235% depending on the metal. This trend is consistent with faster HER kinetics in acidic media, where protons are directly available, compared with alkaline media, where proton supply relies on water [42]. However, for Bi, Ag, Au, and Pd, the relative increase in H_2 generation between pH 1 and 13 is modest (< 38%), indicating that proton availability alone does not fully determine HER activity in NO_3RR systems. Instead, the presence of KNO_3, absent in conventional HER studies, may influence hydrogen evolution during NO_3RR. This is evident from the comparison between Pd and Mo, whose HER activities deviated from expectations based on hydrogen

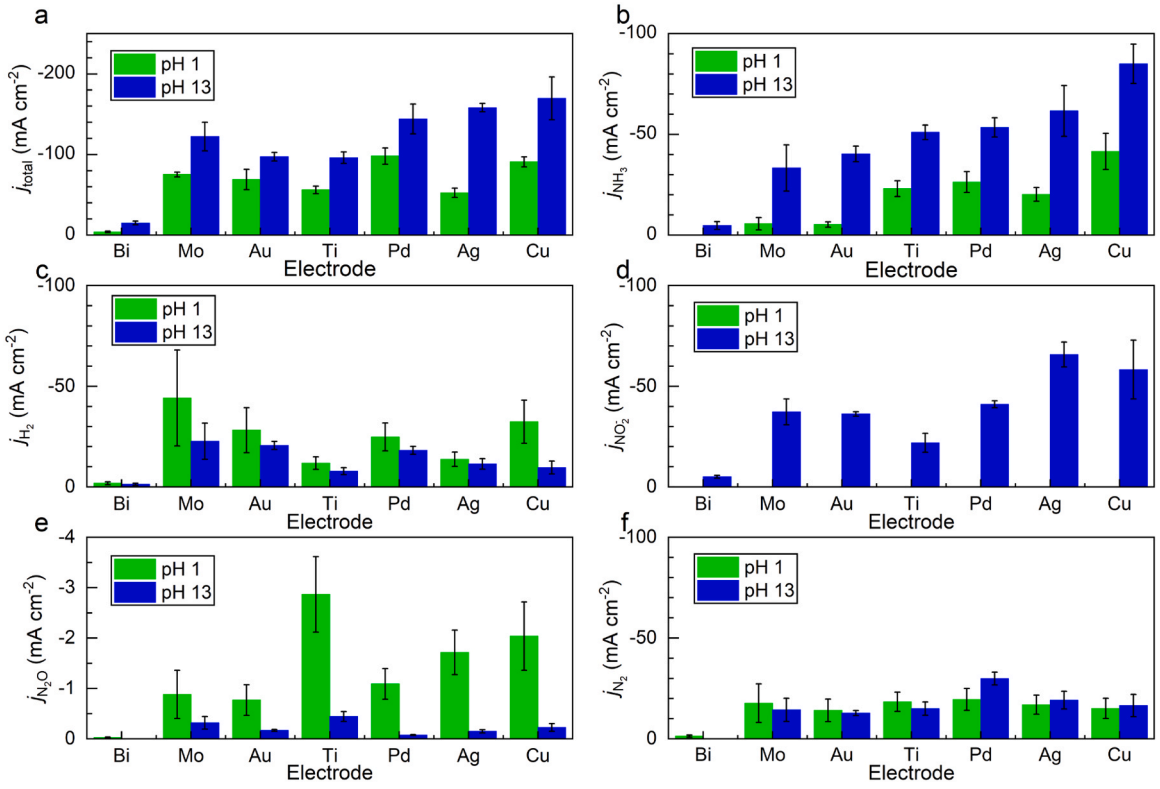

Fig. 1. Effect of electrolyte pH on NO_3RR kinetics evaluated on polycrystalline metals (Bi, Mo, Au, Ti, Pd, Ag, and Cu) electrodes at −0.75 V vs RHE in a 0.3 M NO_3^-. Panel (a) shows total current density (j_{total}), while panels (b–f) show partial current densities (j_i) for NH_3, H_2, NO_2^-, N_2O, and N_2 under acidic (pH 1) and alkaline (pH 13) conditions. Higher total currents and enhanced NH_3 formation are observed under alkaline conditions, highlighting the effect of proton availability on NO_3RR kinetics.

adsorption free energies (ΔG_H) [43–45]. Pd ($\Delta G_H \approx 0$) is typically considered an optimal HER catalyst, whereas Mo binds hydrogen too strongly ($\Delta G_H < 0$), which limits HER activity [43–45]. Contrary to this expectation, Mo exhibited a ~78% higher H_2 formation rate than Pd at pH 1 (-44.13 and −24.75 mA cm^{-2}). A similar trend was observed at pH 13, where Mo still showed slightly higher activity than Pd (-20.3 vs −18.4 mA cm^{-2}, ~ 10% difference). It is noteworthy that Pd formed a Pd hydride (PdH_x) phase under pH 1 conditions (Fig. 2), consistent with previous reports [46,47], whereas no such phase was observed at pH 13. For Mo and the other metals, no bulk structural changes were observed at either pH (Figure S2). While the formation of hydride or other species (e.g., oxide or hydroxide) at the surface cannot be excluded, the presence of oxide or hydroxide is less probable, as metallic phases are favored under cathodic potentials [48,49]. Although reports in the HER literature suggest that PdH_x can enhance H_2 activity [50], its formation did not result in higher j_{H_2} in our NO_3RR systems. These results indicate that the presence of KNO_3 and nitrate reduction itself can alter hydrogen evolution behavior on Pd and Mo (likely on other metals as well, though to a lesser extent) under the applied potential. To further confirm this, control HER experiments for Pd and Mo were performed at pH 1 and in the absence of KNO_3. Under these conditions, Pd exhibited approximately two-fold higher H_2 activity (-85.75 mA cm^{-2}) than Mo (-43.27 mA cm^{-2}; Figure S3), consistent with trends expected from their respective ΔG_H values.

Together, these findings indicate that HER suppression or promotion in NO_3RR systems is strongly influenced by electrolyte pH and the presence of KNO_3, thereby modifying the energetics of HER at the electrodes.

We next consider the formation of NO_3RR by-products. The electrolyte pH strongly influences their formation rate, underscoring the mechanistic sensitivity of NO_3RR to proton availability. As shown in Fig. 1**d**, $j_{NO_2^-}$ were observed exclusively under alkaline conditions,

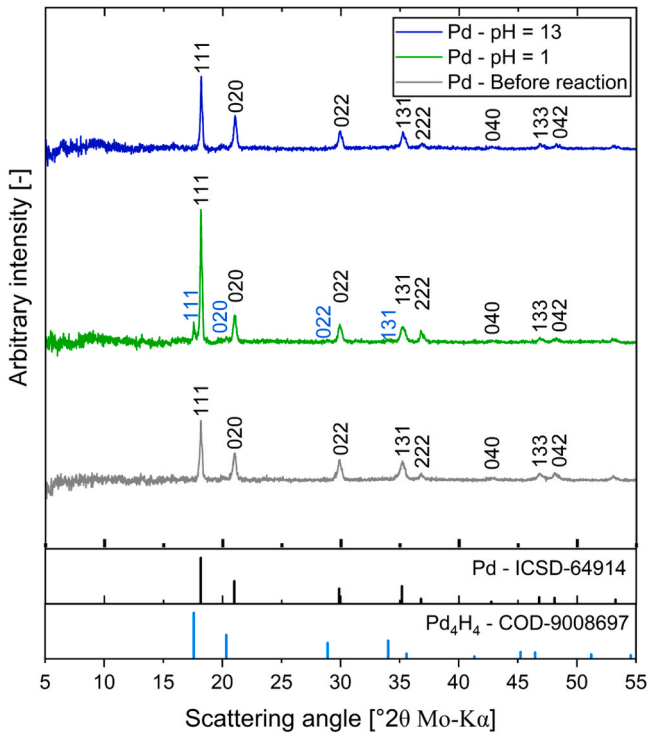

Fig. 2. XRD patterns of Pd electrodes recorded ex situ before (on grey) and after reaction at pH 1 (green) and at pH 13 (blue) at −0.75 V vs RHE. Reference patterns (PDF cards) are included for phase identification. Phase identification suggests PdH_x formation at pH 1.

indicating weak stabilization of NO_{2ads}^{-} on the catalyst surface under such conditions. This weak stabilization increases the probability that NO_{2ads}^{-}, formed in the first step of NO_3RR, desorbs before undergoing further reduction, in agreement with our measured $j_{NO_2^-}$. In contrast, the absence of NO_2^- in acidic electrolytes suggests that the subsequent reduction of NO_{2ads}^{-} to NH_3 or other by-products proceeds sufficiently fast to suppress NO_{2ads}^{-} from desorption. This enhanced apparent reduction kinetics at pH 1 can be associated with the high concentration of hydronium ions (H_3O^+), which provide protons more readily than water, the proton donor in alkaline media, thereby facilitating further reduction of NO_{2ads}^{-}.

N_2O and N_2 were also formed as by-products across all metals (Figs. 1**e and** 1**f**), regardless of the extreme pH conditions (pH 1 and 13). N_2O formation was slow, with j_{N_2O} not exceeding 3.5 mA cm^{-2}; the highest j_{N_2O} values were consistently observed in pH 1 reaction systems, as shown in Fig. 1**e**. Previous mechanistic studies in acidic media have shown that N_2O can form via dimerization of NO_{ads}. Despite the low j_{N_2O} observed here, the detection of N_2O indicates that NO_{ads} dimerization to N_2O_{ads} is not exclusive to acidic environments but can also occur, albeit less favorably, in alkaline media.

All the metals, except Bi, exhibited similar reaction kinetics towards N_2, as reflected by comparable j_{N_2} values of ~20 mA cm^{-2} under acidic conditions (Fig. 1**f**). This observation suggests that a key intermediate in the N_2 formation pathway interacts weakly across these metals, rendering its reduction largely insensitive to metal identity and resulting in comparable reaction rates. Considering that N_2O gas was detected in our experiments, it is plausible to consider that N_2O_{ads} is this intermediate. Therefore, N_2 production under these conditions is consistent with the Vooys–Koper–Chumanov mechanism [51,52].

Conversely, under alkaline conditions, j_{N_2} values differed modestly between metals (Fig. 1**f**), indicating a more pronounced metal dependence. This suggests that in alkaline media, N_2 formation is consistent with pathways that do not involve N_2O_{ads}, such as the Duca-Feliu-Koper mechanism, in which NH_{2ads} is the prior intermediate to N_2 [53]. Nevertheless, while the Duca-Feliu-Koper pathway appears to dominate under alkaline conditions, the Vooys–Koper–Chumanov mechanism cannot be completely excluded, as NO_{ads}, an omnipresent intermediate in NO_3RR, may still undergo dimerization to form N_2O_{ads}, as discussed above.

Taken together, these rate analyses suggest that proton availability in the electrolyte plays a key role in determining NO_3RR reaction pathways by modulating nitrate deoxygenation kinetics, intermediate stability, and protonation (illustrated in Scheme 1, right side). At pH 1, high proton availability appears to facilitate the deoxygenation stages, particularly the reduction of NO_{2ads}^{-}, an intermediate prone to desorption if reduced slowly, thereby ensuring that subsequent reduction steps can proceed. However, while abundant protons provide kinetic advantages in these steps, they can be counterproductive for efficient NH_3 formation, as they drive reduction relatively fast along multiple competing pathways with no clear preference. As a result, strongly acidic electrolytes yield NH_3 formation rates comparable to or lower than those of N_2 (predominant by-product). Moreover, the excess of available protons promotes their reduction to H_2, consuming electrons that could otherwise drive NO_{3ads}^{-} reduction. Conversely, under alkaline conditions, the deoxygenation steps generally proceed more slowly, as evidenced by a pronounced desorption of NO_{2ads}^{-}. The limited proton availability also slows the proton-coupled electron transfer (PCET) in the subsequent reduction steps; however, this moderation is not detrimental. Instead, it may favor the NH_3 formation pathway by promoting stepwise hydrogenation of intermediates, leading to higher NH_3 formation rates relative to N_2.

The observation that alkaline conditions yield significantly higher j_{total} and j_{NH_3} values than acidic media, despite slower kinetics and poorer NO_{2ads}^{-} stability, suggests that the influence of electrolyte pH extends beyond reaction pathway selection to include enhanced NO_3^- adsorption, as illustrated in Scheme 1 and detail discussed in **Section 3.3**. Accordingly, under alkaline conditions, a higher coverage of NO_{3ads}^{-} compensates for the loss of NO_{2ads}^{-} due to desorption and allows the remaining NO_{2ads}^{-} to be protonated at a moderate rate, thereby enabling efficient overall NH_3 formation.

Product distribution analysis provided further insight into the effect of electrolyte pH on NO_3RR. First, it confirms that NO_3RR favors NH_3 formation under alkaline conditions relative to acidic ones, as illustrated in Figs. 3**a and** 3**b**. Mo and Au exhibit the most pronounced changes, with Faradaic efficiencies for NH_3 increasing by up to a factor of 5 in alkaline electrolytes. Second, it reveals that high proton concentrations may also promote chemical (non-electrochemical) reactions, resulting in total Faradaic efficiencies below 100% as those observed in Fig. 3**a**. We attribute the missing FE primarily to NO_2 chemical formation, which is favored in acidic media [13] and which is not detected by GC under the present experimental conditions.

Overall, our results demonstrate that electrolyte pH alone exerts a significant and systematic influence on the activity, selectivity, and reaction pathways of NO_3RR. Highly acidic electrolytes promote fast reduction kinetics across the different NO_3RR stages due to high proton availability; however, this comes at the expense of NH_3 selectivity, as it favors the formation of N_2, H_2, and NO_2. In contrast, high alkaline electrolytes reduce the formation of such undesirable products as a

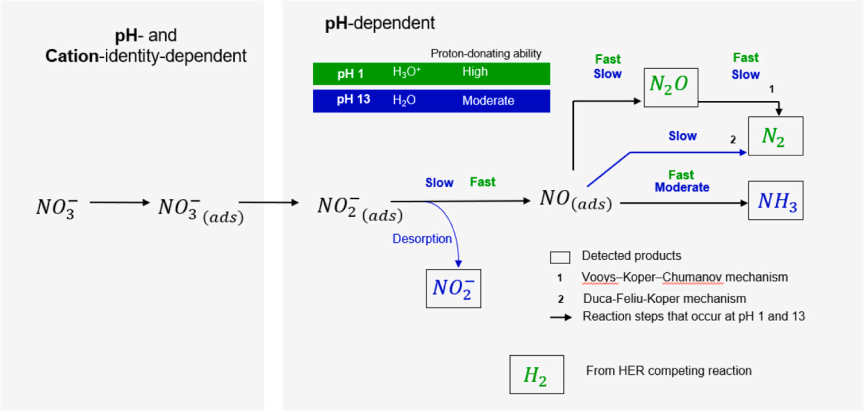

Scheme 1. Simplified representation of the overall NO_3RR process illustrating that electrolyte pH is a key parameter on preferential reaction pathways and nitrate adsorption. High proton availability at pH 1 accelerates the reaction steps, stabilizing the NO_{2ads}^{-} intermediate and favoring N_2 over NH_3, consequently. Proton abundance also promotes HER. Consequently, acidic conditions favor j_{H_2}, j_{N_2O} and j_{N_2}. Conversely, limited proton availability under alkaline conditions slows overall reaction kinetics; with the drawback of NO_2^- desorption but moderate NH_3 formation. Thus, alkaline media favor higher partial current densities for NH_3 and NO_2^-. Electrolyte pH is also critical for nitrate adsorption along with cation identity. Electrons and protons involved in the elementary steps are omitted for clarity.

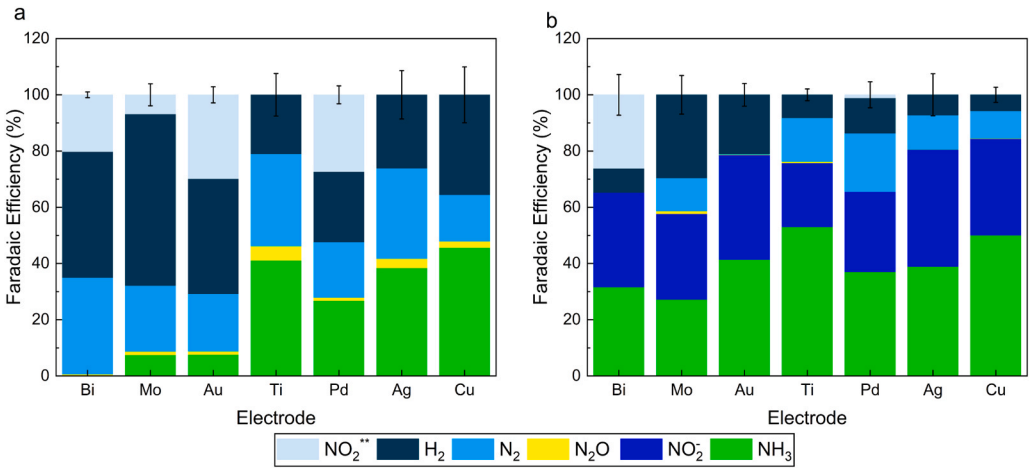

Fig. 3. Effect of electrolyte pH on NO_3RR product selectivity assessed on polycrystalline metals (Bi, Mo, Au, Ti, Pd, Ag, and Cu) electrodes at −0.75 V vs RHE in a 0.3 M NO_3^-. Product selectivity, expressed as Faradaic efficiency (FE, %), is shown for (a) acidic conditions (pH 1) and (b) alkaline conditions (pH 13). Error bars represent the SD of the FE_{total} from three independent electrolysis experiments. ** indicates that it was chemcially formed.

consequence of more restricted proton availability, which moderates NO_3RR kinetics in a manner that promotes higher NH_3 formation rates and enhanced selectivity. Furthermore, our results suggest that NO_3^- adsorption is also sensitive to electrolyte pH as discussed in **Section 3.3**.

3.2. Interplay between applied potential and electrolyte pH

Potentiostatic electrolysis was performed between −0.25 and −1.00 V vs RHE to determine whether the observed pH-dependent trends described above are influenced by applied potential. For this purpose, Cu, Ti, and Pd were selected as representative electrodes because they exhibited distinct activities toward ammonia formation and the competing HER at a fixed potential of −0.75 V vs RHE (**Section 3.1**). Cu was the most active for NH_3 formation, whereas Ti and Pd showed moderate NO_3RR activity but contrasting HER behavior (limited on Ti and strong on Pd) as shown in Fig. 1. This diversity in activity is essential for distinguishing intrinsic catalyst-driven behavior from effects arising from the interplay between applied potential and electrolyte pH.

The lower potential limit (-0.25 V vs RHE) was chosen to be more cathodic than the operational onset potential of the electrochemical systems, defined here as the potential required to reach −1 mA cm^{-2}, thereby ensuring operation within an electrochemically active regime. Interestingly, the NO_3RR onset of measurable cathodic current occurs at more negative potentials in acidic media than in alkaline electrolytes (Figure S4), even when referenced to RHE. For example, the operational NO_3RR onset potential shifts by ~112–340 mV to more negative values in acidic media compared to alkaline conditions (Table S1). This behavior suggests that proton availability alone may not be sufficient to lower the kinetic barrier for NO_3RR initiation and may instead delay its apparent onset due to stronger competition from HER and poor NO_3^- adsorption, as is further discussed in **Section 3.3**.

As shown in Fig. 4**a,** the j_{total} increases with more negative potential for all three metals, reflecting the enhanced electron-transfer rate driven by a higher overpotential. Importantly, the relative effect of electrolyte pH on j_{total} remains essentially unchanged across the investigated potential window, with significantly higher current densities observed under alkaline conditions. These results indicate that while the applied potential governs the driving force for interfacial electron transfer, the efficiency of electron utilization in NO_3RR is strongly modulated by electrolyte pH, with alkaline conditions promoting higher overall j_{total} and increased NH_3 formation rates.

The impact of electrolyte pH on electron utilization is further reflected in the partial current densities toward individual products, providing insight into reaction pathway preferences. Across the entire potential range, alkaline conditions consistently promote higher j_{NH_3}, and $j_{NO_2^-}$ than acidic conditions (Figs. 4**b and** 4**c**). In contrast, acidic electrolytes favor higher j_{H_2}, j_{N_2}, and j_{N_2O} (Fig. 4**d–f**). These observations indicate that electrolyte pH establishes preferential NO_3RR pathways by controlling stability of key intermediates and proton availability for effective protonation, and that these pathways are largely preserved across the examined potential window, particularly under alkaline conditions.

While electrolyte pH largely governs the dominant reaction pathways, the applied potential significantly modulates how these pathways are expressed, i.e., the relative product selectivity arising from each pathway. For Cu (Fig. 5) and similarly for Ti and Pd (Figure S5), two distinct trends in NH_3 Faradaic efficiency (FE_{NH_3}) emerge depending on the electrolyte pH. Under acid conditions, FE_{NH_3} reaches a maximum at −0.5 V vs RHE and decreases at more cathodic potentials (−0.75 and −1.00 V vs RHE) as shown in Fig. 5**a**. Such a decline correlates with an increase in FE_{H_2} and FE_{NO_2} at −0.75 and −1.00 V vs RHE, respectively. This behavior indicates that while moderate cathodic potentials favor NH_3 formation, increasingly negative potentials promote competing reduction pathways in acidic media. Conversely, under alkaline conditions, FE_{NH_3} increases monotonically with cathodic potential, accompanied by a decrease in $FE_{NO_2^-}$ (Fig. 5**b**), suggesting that a larger fraction of NO_{2ads}^- intermediates undergo reduction rather than desorption.

Taken together, these results demonstrate that electrolyte pH primarily governs the dominant NO_3RR pathways by controlling intermediate stability and modulating protonation rate effectively, whereas the applied potential modulates the extent to which these pathways are expressed, ultimately shaping product selectivity. This distinction highlights the complementary roles of pH and applied potential: pH sets the mechanistic landscape of NO_3RR, while potential establishes the driving force for interfacial electron transfer and tunes relative expression of competing pathways.

3.3. Effect of KNO_3 concentration

To further elucidate the effect of the electrolyte on NO_3RR, we investigated how KNO_3 concentration influences ammonia formation across applied potentials at pH 1 and 13. The combined effects of these variables on the ammonia partial current density (j_{NH_3}) are presented as heat maps in Fig. 6. Green and blue color scales correspond to pH 1 and pH 13, respectively, with darker shades indicating higher current densities. The study was conducted on Pd, Ti, and Cu electrodes, following their established use in the preceding experiments and enabling direct

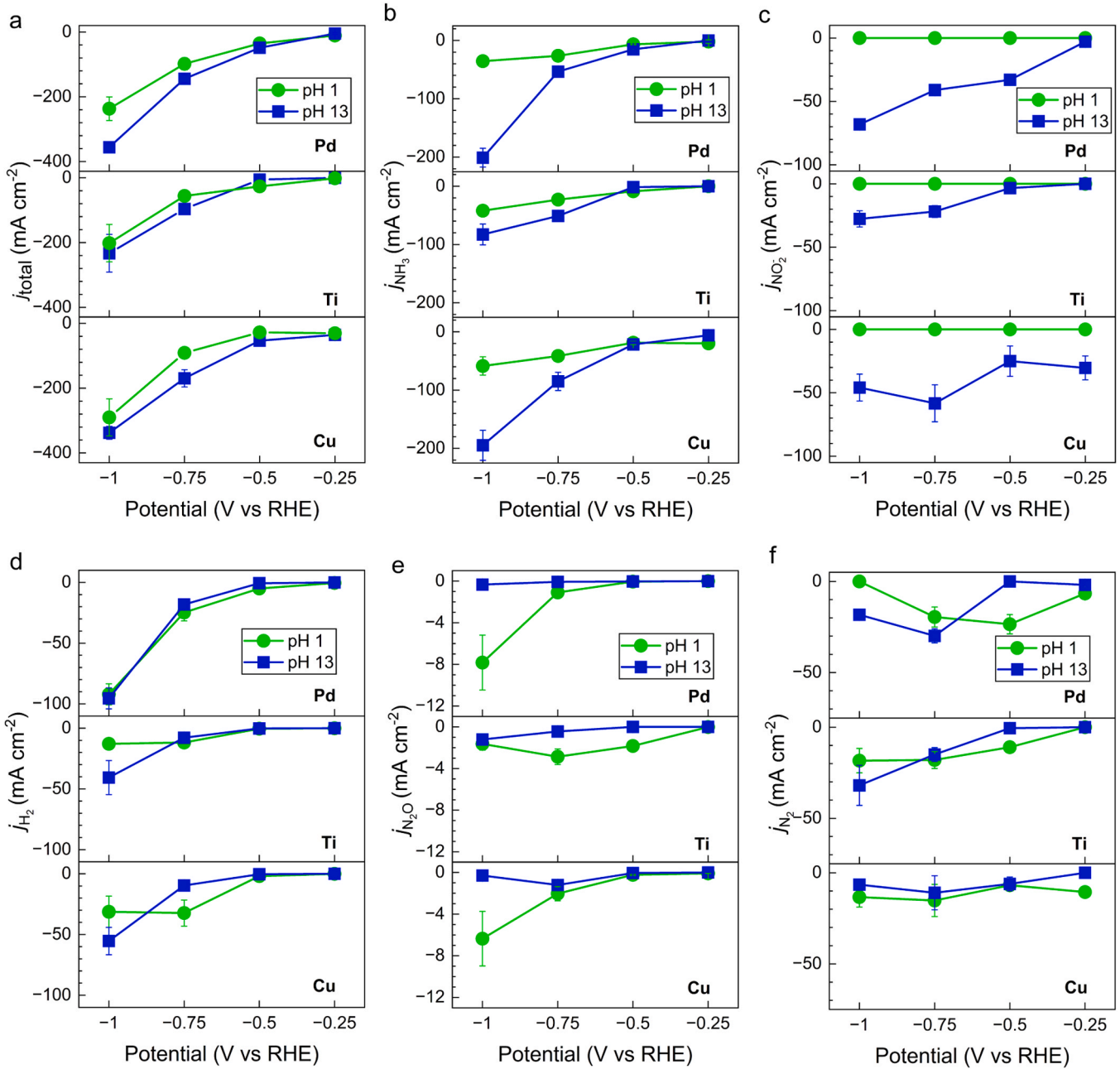

Fig. 4. Comparison of electrochemical activity as a function of applied potential (V vs RHE) for NO_3RR under acidic and alkaline conditions. Panel (a) shows total current density (j_{total}), while panels (b–f) show partial current densities (j_i) for NH_3, NO_2^-, H_2, N_2O, and N_2. Measurements were performed on Pd, Ti, and Cu electrodes in electrolytes containing 0.3 M NO_3^- at pH 1 and pH 13 over the potential range −0.25 to −1.00 V vs RHE. Increasingly cathodic potential enhances overall activity, while the magnitude of this enhancement is strongly modulated by electrolyte pH, with alkaline conditions being more favorable.

comparison of trends across different metal surfaces.

The effect of pH on NO_3RR toward NH_3 is consistent across the experimental parameter space shown in Fig. 6. For the three metals, the heat maps reveal systematically higher j_{NH_3} at pH 13 than at pH 1, confirming that ammonia formation is favored under alkaline conditions.

Beyond this clear pH effect, a more detailed analysis of the heat maps provides additional insights into NO_3RR behavior. Examining the heat maps at a fixed potential along the vertical axis, j_{NH_3} shows little dependence on nitrate concentration at pH 1, a behavior most clearly seen for Pd and Ti (Fig. 6**a and b**). In contrast, at pH 13, j_{NH_3} increases monotonically with nitrate concentration across all electrodes (Fig. 6**d-f**). These trends indicate that nitrate concentration strongly influences NO_3RR activity toward NH_3 under alkaline conditions, whereas its influence is substantially weaker in acidic media.

The observed behavior can be rationalized as follows. Under cathodic polarization, the negatively charged electrode repels anions (hydroxide at pH 13 and nitrate at both pH 1 and 13), leading to their local depletion, while simultaneously attracting cations (protons at pH 1 and potassium at both pH 1 and 13), resulting in their accumulation near the electrode, as is illustrated in Scheme 2**a**. However, the distribution of cations near the electrode differs markedly between acidic and alkaline conditions, as is shown in Scheme 2**b and c**. At pH 1, proton adsorption is favored over K^+ not only due to their higher availability but also because of the stability of the adsorbed protons. Unlike K^+, which retains a partial positive charge upon adsorption (see Eq. 2) [54–56], and thus experiences repulsive interactions between $K_{ads}^{(1-\delta)}$ that limit surface

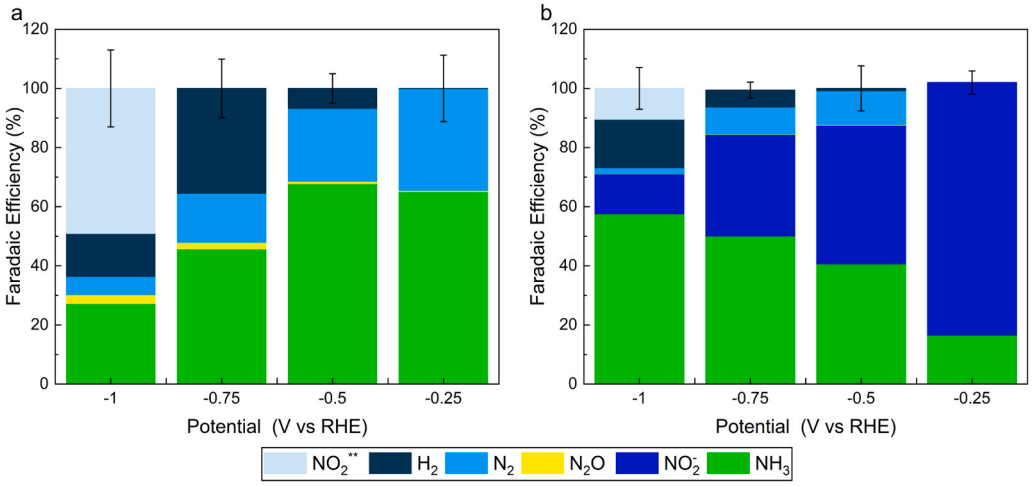

Fig. 5. Influence of applied potential on NO_3RR selectivity evaluated under acidic (a) and alkaline (b) conditions. Measurements were performed on Cu electrodes in electrolytes containing 0.3 M NO_3^- at pH 1 and 13 within the potential range −0.25 to −1.00 V vs RHE. Error bars represent the SD of the FE_{total} from three independent electrolysis experiments.

coverage, protons undergo full electron transfer to form neutral H atoms (H_{ads}, see Eq. 3) [54], enabling stable adsorption. Consequently, while H_{ads} covers the metal surface, K^+ ions are primarily electrostatically adsorbed (i.e., without direct contact with the surface electrode) in the Outer Helmholtz Plane (OHP) [54]. The localized K^+, at the OHP, generates a strong electric field that draws NO_3^- ions from the bulk solution to the OHP, thereby helping overcome the natural repulsion between NO_3^- and the cathode and allowing nitrate access to the reactive region. However, the extent to which nitrate reaches the surface depends on the availability of active sites, which at pH 1 are largely occupied by H_{ads}. Thus, an increase in NO_3^- concentration at the OHP does not affect the reaction when surface availability is the limiting factor. This explains why ammonia formation was poorly sensitive to electrolyte concentration at pH 1.

$$K^+_{(aq)} + \quad * + \quad \delta e^- \quad \leftrightharpoons K^{(1-\delta)}_{ads} \tag{2}$$

$$H^+_{(aq)} + \quad * + \quad \delta e^- \quad \leftrightharpoons H_{ads} \tag{3}$$

At pH 13, the specific adsorption (i.e., chemically bonded to the surface and partially discharged [35,56,57]) of K^+ is promoted by weak competition with H^+ due to the low proton concentration. Although more K^+ ions are adsorbed under these conditions, full surface coverage is not attained because their residual positive charge induces repulsion between neighboring $K^{(1-\delta)}_{ads}$. This residual charge, however, attracts NO_3^- from the OHP toward the electrode, which in this case presents more available surface sites for NO_3^- adsorption. K^+ ions attracted to the negatively charged electrode but not specifically adsorbed accumulate in the OHP, which in turn facilitates NO_3^- enrichment in this region. As the electrolyte concentration increases, more K^+ ions can be electrostatically stabilized at the OHP, enabling a higher flux of NO_3^- to reach the reaction region and favoring its electrochemical reduction. Consistent with this explanation, the heat maps of the three metals at pH 13 (Fig. 6**d-f**) clearly show that ammonia formation increases with electrolyte concentration, revealing that cations are not passive spectators but actively influence NO_3^- reduction.

When the heat maps are examined along the potential axis, the influence of the applied potential on ammonia formation becomes apparent. As shown in Fig. 6, independent of electrolyte pH, the ammonia partial current density increases with increasingly cathodic potentials, reaching maximum values at −1.0 V and minimum values at −0.25 V vs RHE across nearly all nitrate concentrations. Notably, the magnitude of the increase in j_{NH_3} with increasingly cathodic potential is substantially larger under alkaline conditions (Fig. 6**d-f**). This behavior can be explained not only by the higher thermodynamic driving force for electron transfer at more negative potentials, but also by changes in the interfacial electric field. Stronger cathodic polarization enhances the electric field at the interface, which attracts more K^+ ions to the OHP. The increased local K^+ concentration promotes NO_3^- enrichment near the electrode surface, thereby increasing its availability for reduction. The effect is more pronounced under alkaline conditions, where low proton concentration minimizes competition for surface sites and allows the formation of a K^+-rich interfacial structure. As a result, more nitrate reaches the surface, further enhancing ammonia formation.

The higher interfacial NO_3^- availability also facilitates its rapid adsorption and accelerates the formation of the first reduced intermediate (NO_2^-). This promotes earlier initiation of reaction, consistent with the shift toward less negative NO_3RR onset potential observed in alkaline media (Figure S4).

Overall, the heat map analysis shows that KNO_3 concentration strongly affects NH_3 formation under alkaline conditions but has little impact in acidic media. This behavior may be related to changes in interfacial K^+ structure: higher KNO_3 concentrations promote K^+ accumulation at the interface, increasing NO_3^- availability in the reaction region. In acidic conditions, high proton concentration diminishes this effect and blocks surface sites. More negative potentials further enhance interfacial K^+ accumulation, favoring NO_3^- conversion in alkaline electrolytes. Importantly, the analysis suggests that alkali metal cations play a significant role as electric-field mediators in the NO_3RR, and the observed increase in activity with KNO_3 concentration —more pronounced at pH 13— may not be only to nitrate levels, but also to K^+ levels, which help to nitrates to reach the electrode surface.

3.4. *Influence of co-existing cations*

To verify that the KNO_3 concentration-dependent activity observed is driven mainly by cation participation rather than by the sole increase of nitrate concentration, we replaced K^+ with Cs^+ at the three electrolyte concentrations in both alkaline and acidic conditions. K^+ and Cs^+ have different ionic radii and hydration structures [58,59]. These differences are expected to alter the cation's ability to mediate the interfacial electric field between the electrode and nitrate ions under applied potential, thereby influencing the rate of ammonia formation. To ensure consistency with previous results, the experiments were conducted on Ti, Cu, and Pd. Because the effect of concentration was more pronounced under alkaline conditions (as shown in Fig. 6 of the previous section), all three metals were evaluated at pH 13, while acidic conditions were

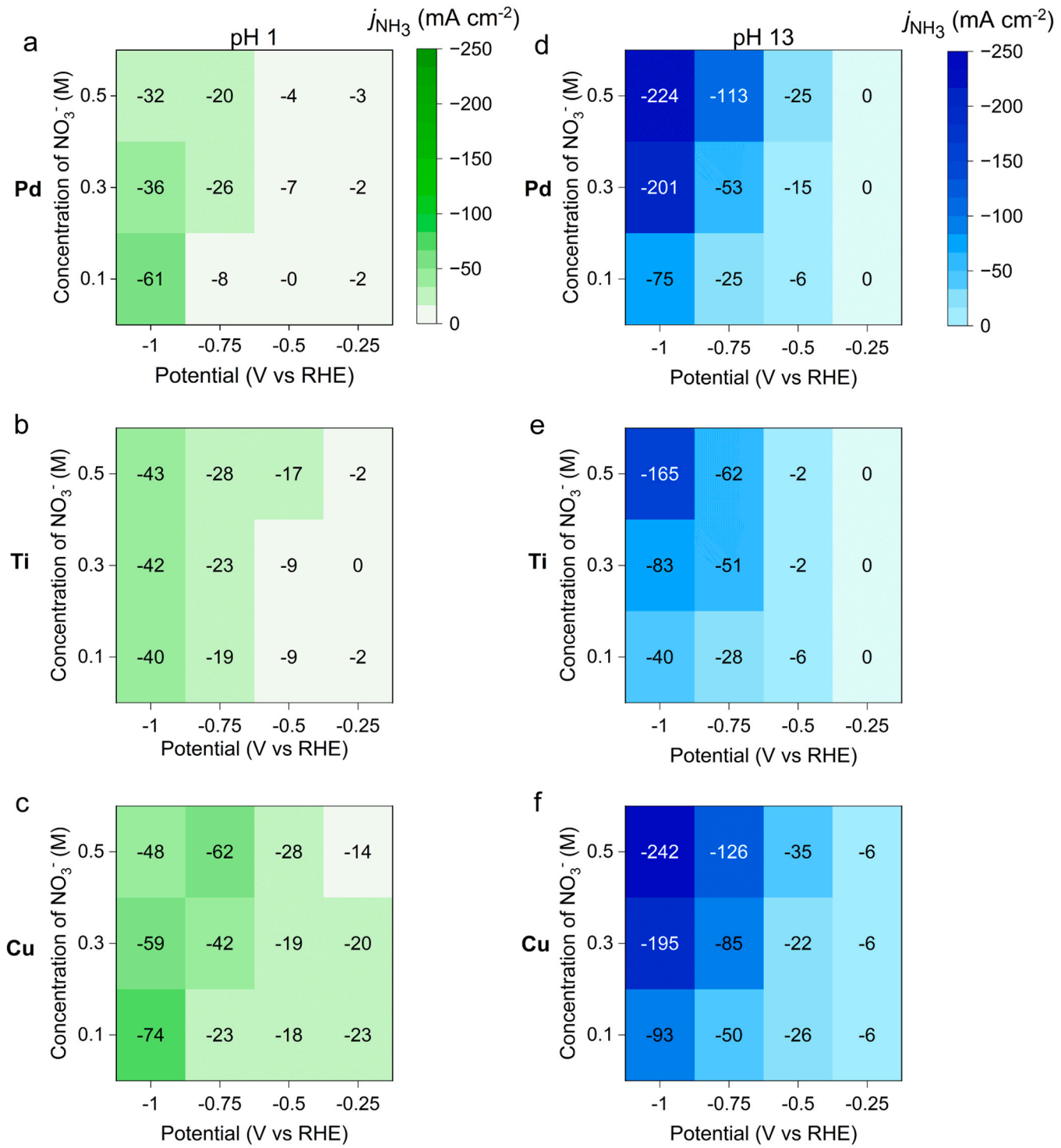

Fig. 6. Heatmaps of ammonia partial current density j_{NH_3} as a function of applied potential and nitrate concentration at pH 1(left) and pH 13 (right) for Pd, Ti, and Cu. Each grid square displays a one-hour potentiostatic experiment under the specified pH, nitrate concentration, and applied potential.

investigated using Ti as the representative system. A potential of −0.75 V vs RHE was applied.

Fig. 7 shows that j_{NH_3} increases at all concentrations when K^+ is replaced with Cs^+. As expected, this effect is more pronounced in alkaline than in acidic media, as illustrated for Ti electrodes. On average, substituting K^+ with Cs^+ enhances j_{NH_3} by ∼36% in acidic conditions and ∼59% in alkaline conditions (Fig. 7 **a and b**). A similar trend is observed for Cu and Pd, which exhibited increases of ∼32% and ∼140% in ammonia formation rates in alkaline media, respectively (Fig. 7 **c and d**). These results are consistent with the findings of Fajardo et al., who reported enhanced NO_3^- removal in the presence of Cs^+ during NO_3RR on Sn electrodes in alkaline media [60]. Therefore, our results demonstrate not only that cations actively participate in NO_3RR, but also that the magnitude of their influence depends on cation identity. Our mechanistic interpretation, based on the overall trends observed in this work, is that alkali cations in NO_3RR influence the interfacial electric field, facilitating the approach of NO_3^- to the negatively polarized surface. The enhanced j_{NH_3} observed with Cs^+

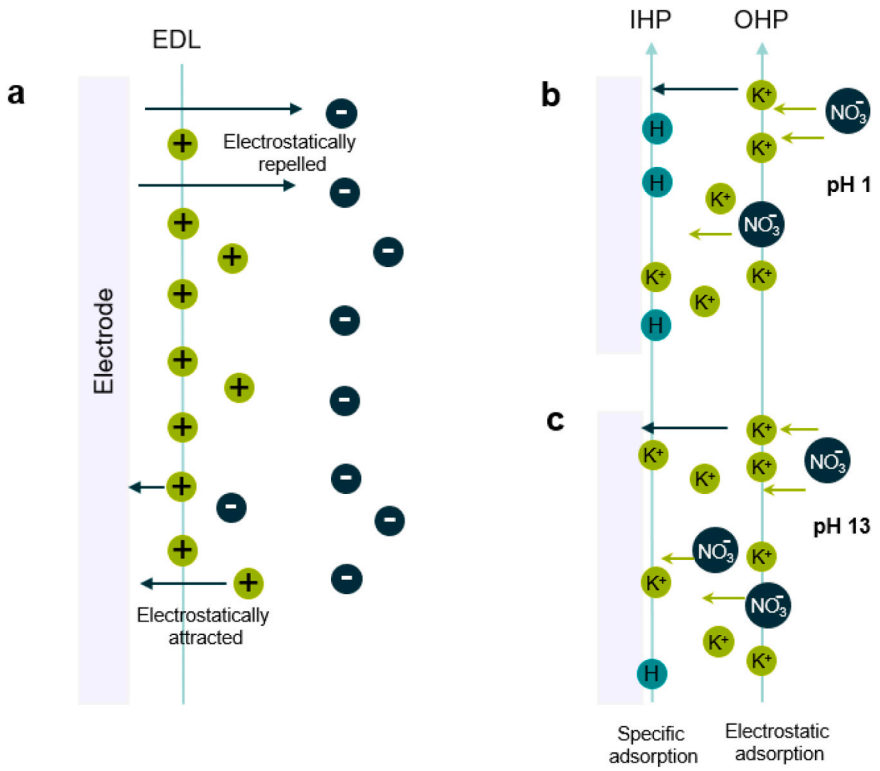

Scheme 2. Schematic illustration of the ion distribution in the electrical double layer (EDL) under a cathodic potential. Cation species are electrostatically attracted to the negatively charged electrode, while the anions are repelled, resulting in an EDL enriched in cations **(a)**. Refined views of the EDL structure of NO_3RR electrolytes at pH 1 **(b)** and pH 13 **(c)** show the specific and electrostatic adsorption of the cations at the inner and outer Helmholtz planes (IHP and OHP), respectively. Protons (H^+) undergo full electron transfer upon specific adsorption, forming electrically neutral $H_{ads.}$ In contrast, alkali metal cations, exemplified by K^+, remain positively charged upon adsorption at the IHP. Thus, K^+ at IHP and OHP generates a positive electric field that attracts nitrates close to the surface, screening the inherent electrostatic repulsion between the negatively charged electrode and nitrate. At pH 13, more electrode surface is available since K^+ coverage is low due to its remaining charge.

suggests that Cs^+ is a more effective mediator than K^+, particularly in alkaline media, where the absence of protons reduces competition for adsorption sites.

Alkali metal cations also influence the competing HER, although in a more complex manner than NO_3RR. For HER, the cation effect varies with the electrode material. In the case of Ti, the presence of Cs^+ leads to a decrease in j_{H_2} of ~61% under acidic conditions and ~21% under alkaline conditions relative to with K^+ (Fig. 7 **a and b**). For Cu and Pd (Figs. 7**c and** 7**d**), Cs^+ enhanced j_{H_2} by a ~24% and ~56% with respect to K^+, respectively. This variation in the effect of alkali cations on the metal is consistent with previous HER studies [38,61]. For example, Bender et. al. reported that HER rates increase with cation size ($Li^+ < Na^+ < K^+ < Cs^+$) over Cu, Ag, and Au, whereas the opposite is observed on Ir and Pt [61]. The origin of this variation lies beyond the scope of this work. However, it is important to note that, regardless of whether the HER activity increases or decreases with alkali cations on different metals, the rate remains significantly lower than the NH_3 formation rate.

Thus, these experiments confirm that alkali cations participate in NO_3RR, acting as electric-field mediators that help overcome the intrinsic electrostatic repulsion between the negatively polarized electrode and NO_3^- .The extent of this effect depends on both cation identity and electrolyte pH for NO_3RR.

4. Conclusion

We investigated how and to what extent the electrolyte properties (concentration, pH, and co-existing ions), together with the applied potential, influence NO_3RR towards NH_3. Systematic studies on multiple metal electrodes allowed us to disentangle intrinsic catalyst behavior from electrolyte-induced effects. We found that electrolyte pH strongly influences NO_3RR activity, with alkaline conditions favoring higher j_{total} and j_{NH_3} under comparable driving forces. Our pH studies showed that the availability of protons in the bulk electrolytes also directs NO_3RR along preferential reaction pathways. At pH 13, the pathways towards NH_3 and NO_2^- formation are favored over those leading to N_2, N_2O and H_2, whereas acidic conditions promote N_2, N_2O and H_2 formation. These pH-dependent trends persist across the studied potential range (-0.25–1.00 V vs RHE). While electrolyte pH defines the dominant reaction pathways, the applied potential modulates their relative contributions, determining product selectivity.

Furthermore, we show that the initial NO_3^- concentration influences the NH_3 formation rate only under alkaline conditions, whereas its impact is negligible under acidic conditions. Our results indicate that NO_3^- concentration is closely associated with the presence of co-existent alkali metal cations. The results suggest that these cations act as electrostatic field mediators, mitigating the intrinsic repulsion between the negatively polarized electrode and NO_3^-, thereby electrostatically attracting them to the electrode surface for effective conversion to ammonia. The effectiveness of a given cation as a mediator is a function of the pH, applied potential, concentration, and identity of the cation.

Overall, our results demonstrate that the electrolyte alone exerts a systematic and decisive influence on NO_3RR activity and reaction pathways, providing an integrated understanding of how specific electrolyte properties contribute and interact during nitrate-to-ammonia conversion. These findings offer a framework for engineering electrolytes for NO_3RR and call for redefining alkali metal cations from spectator species to active mediators.

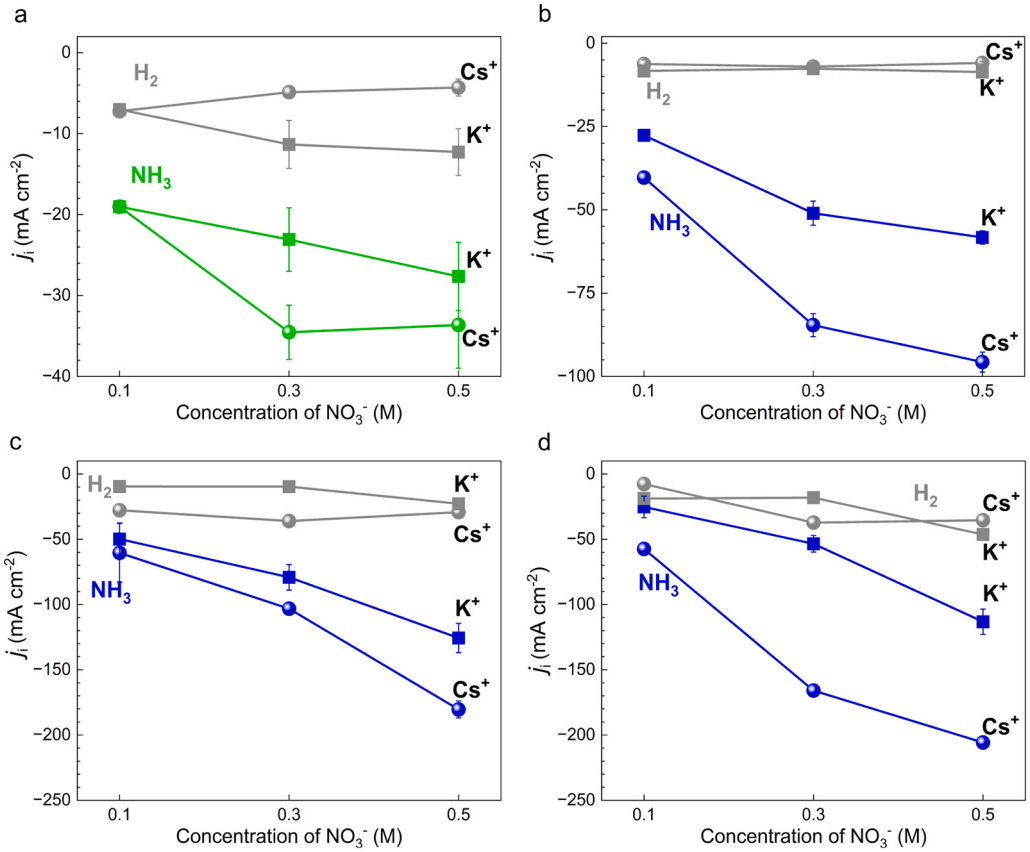

Fig. 7. Effect of cation identity on NH_3 and H_2 activity. The influence of alkali cations on j_{NH_3} and j_{H_2} under acidic (a) and alkaline (b) conditions is illustrated using Ti as electrode. Cu (c) and Pd (d) show the corresponding behaviour under alkaline conditions. All experiments were conducted at −0.75 V vs RHE for 1 h under stirring at 300 rpm.

Declaration of Competing Interest

The authors declare that they have no known competing financial interests or personal relationships that could have appeared to influence the work reported in this paper.

Acknowledgments

The financial support by the German Federal Ministry of Research, Technology, and Space (BMFTR) under the project iNew2.0 (FKZ 03SF0627A) is gratefully acknowledged.

Appendix A. Supporting information

Supplementary data associated with this article can be found in the online version at doi:10.1016/j.apcatb.2026.127017.

Data availability

Data will be made available on request.

References

[1] G. Sundermann, N. Wägner, A. Cullmann, C. Von Hirschhausen, C. Kemfert, Nitrate pollution of groundwater long exceeding trigger value; fertilization practices require more transparency and oversight, DIW Wkly. Rep. 10 (2020), https://doi.org/10.18723/diw_dwr:2020-9-1.

[2] M.H. Ward, R.R. Jones, J.D. Brender, T.M. de Kok, P.J. Weyer, B.T. Nolan, C. M. Villanueva, S.G. van Breda, Drinking water nitrate and human health: An updated review, Int. J. Environ. Res. Public Health 15 (2018), https://doi.org/10.3390/ijerph15071557.

[3] E. Abascal, L. Gómez-Coma, I. Ortiz, A. Ortiz, Global diagnosis of nitrate pollution in groundwater and review of removal technologies, Sci. Total Environ. 810 (2021), https://doi.org/10.1016/j.scitotenv.2021.152233.

[4] M. Gutiérrez, R.N. Biajioni, Alarcón-Herrera Maria Teresa, B.A. Rivas-Lucero, An overview of nitrate sources and operating processes in arid and semiarid aquifer systems, Sci. Total Environ. 624 (2017) 1513–1522, https://doi.org/10.1016/j.scitotenv.2017.12.252.

[5] D. Tonelli, L. Rosa, P. Gabrielli, A. Parente, F. Contino, Cost-competitive decentralized ammonia fertilizer production can increase food security, Nat. Food 5 (2024) 469–479, https://doi.org/10.1038/s43016-024-00979-y.

[6] M. Asami, R.J. Bevan, J. Cotruvo, A. Eckhardt, J.K. Fawell, M. Giddings, P. Marsden, Y. Matsui, M.E. Meek, E. Ohanian, C.N. Ong, R. Ramasamy, S. Snyder, Nitrate and Nitrite in Drinking-water: Background document for development of WHO Guidelines for Drinking-water Quality, 2016. ⟨http://www.who.int/publications/guidelines/⟩.

[7] C. Gabaldón, M. Izquierdo, V. Martínez-Soria, P. Marzal, J.M. Penya-roja, F. Javier Alvarez-Hornos, Biological nitrate removal from wastewater of a metal-finishing industry, J. Hazard. Mater. 148 (2007) 485–490, https://doi.org/10.1016/j.jhazmat.2007.02.071.

[8] R. Marecik, R. Biegańska-Marecik, P. Cyplik, Ł. Ł, awniczak, Ł. Chrzanowski, Phytoremediation of Industrial Wastewater Containing Nitrates, Nitroglycerin, and Nitroglycol, Pol. J. Environ. Stud. 22 (2013) 773–780.

[9] G. Zhang, B. Li, Y. Shi, Q. Zhou, W.J. Fu, G. Zhou, J. Ma, S. Yin, W. Yuan, S. Miao, Q. Ji, J. Qu, H. Liu, Ammonia recovery from nitrate-rich wastewater using a membrane-free electrochemical system, Nat. Sustain 7 (2024) 1251–1263, https://doi.org/10.1038/s41893-024-01406-7.

[10] P.H. Van Langevelde, I. Katsounaros, M.T.M. Koper, Electrocatalytic Nitrate Reduction for Sustainable Ammonia Production, Joule 5 (2021) 290–294, https://doi.org/10.1016/j.joule.2020.12.025.

[11] W. Zhong, Z. Gong, P. Chen, Q. Cao, X. Liu, Y. Chen, Z. Lin, Electrochemical reduction of nitrate to ammonia: From fundamental understanding to practical applications, Chem. Catal. 4 (2024), https://doi.org/10.1016/j.checat.2024.101060.

[12] N. Hoang Truong, J.S. Kim, J. Lim, H. Shin, Electrochemical reduction of nitrate to Ammonia: Recent progress and future directions, Chem. Eng. J. 495 (2024), https://doi.org/10.1016/j.cej.2024.153108.

[13] D. Anastasiadou, Y. van Beek, E.J.M. Hensen, M. Costa Figueiredo, Ammonia electrocatalytic synthesis from nitrate, Electrochem. Sci. Adv. 3 (2023), https://doi.org/10.1002/elsa.202100220.

[14] J. Lim, C.A. Fernández, S.W. Lee, M.C. Hatzell, Ammonia and Nitric Acid Demands for Fertilizer Use in 2050, ACS Energy Lett. 6 (2021) 3676–3685, https://doi.org/10.1021/acsenergylett.1c01614.

[15] R.C. Scholes, M.A. Vega, J.O. Sharp, D.L. Sedlak, Nitrate removal from reverse osmosis concentrate in pilot-scale open-water unit process wetlands, Environ. Sci. (Camb. 7 (2021) 650–661, https://doi.org/10.1039/d0ew00911c.

[16] J.W. Palko, D.I. Oyarzun, B. Ha, M. Stadermann, J.G. Santiago, Nitrate removal from water using electrostatic regeneration of functionalized adsorbent, Chem. Eng. J. 334 (2017) 1289–1296, https://doi.org/10.1016/j.cej.2017.10.161.

[17] J.M. McEnaney, S.J. Blair, A.C. Nielander, J.A. Schwalbe, D.M. Koshy, M. Cargnello, T.F. Jaramillo, Electrolyte engineering for efficient electrochemical nitrate reduction to ammonia on a titanium electrode, ACS Sustain. Chem. Eng. 8 (2020) 2672–2681, https://doi.org/10.1021/acssuschemeng.9b05983.

[18] J. Guo, M.J. Liu, C. Laguna, D.M. Miller, K.S. Williams, B.D. Clark, C. Muñoz, S. J. Blair, A.C. Nielander, T.F. Jaramillo, W.A. Tarpeh, Electrodialysis and nitrate reduction (EDNR) to enable distributed ammonia manufacturing from wastewaters, Energy Environ. Sci. 17 (2024) 8787–8800, https://doi.org/10.1039/d4ee03002h.

[19] Z. Wang, D. Richards, N. Singh, Recent discoveries in the reaction mechanism of heterogeneous electrocatalytic nitrate reduction, Catal. Sci. Technol. 11 (2021) 705–725, https://doi.org/10.1039/d0cy02025g.

[20] J. Zhou, S. Gao, G. Hu, Recent Progress and Perspectives on Transition Metal-Based Electrocatalysts for Efficient Nitrate Reduction, Energy Fuels 38 (2024) 6701–6722, https://doi.org/10.1021/acs.energyfuels.4c00415.

[21] L. Bai, F. Franco, J. Timoshenko, C. Rettenmaier, F. Scholten, H.S. Jeon, A. Yoon, M. Rüscher, A. Herzog, F.T. Haase, S. Kühl, S.W. Chee, A. Bergmann, R.C. Beatriz, Electrocatalytic Nitrate and Nitrite Reduction toward Ammonia Using Cu2O Nanocubes: Active Species and Reaction Mechanisms, J. Am. Chem. Soc. 146 (2024) 9665–9678, https://doi.org/10.1021/jacs.3c13288.

[22] S. Zhang, J. Wu, M. Zheng, X. Jin, Z. Shen, Z. Li, Y. Wang, Q. Wang, X. Wang, H. Wei, J. Zhang, P. Wang, S. Zhang, L. Yu, L. Dong, Q. Zhu, H. Zhang, J. Lu, Fe/Cu diatomic catalysts for electrochemical nitrate reduction to ammonia, Nat. Commun. 14 (2023), https://doi.org/10.1038/s41467-023-39366-9.

[23] L.M. Wilder, T.J. Aubry, C.S. Gerke, O.Q. Carvalho, J.R. Thurston, M.F. Toney, M. A. Smeaton, J. van de Lagemaat, E.M. Miller, Nitrate-to-Ammonia Electroconversion at Neutral pH on Polycrystalline Vanadium Sulfide Derived from Vanadium Disulfide, ACS Appl. Energy Mater. 8 (2025) 9407–9418, https://doi.org/10.1021/acsaem.5c01047.

[24] K. Fan, W. Xie, J. Li, Y. Sun, P. Xu, Y. Tang, Z. Li, M. Shao, Active hydrogen boosts electrochemical nitrate reduction to ammonia, Nat. Commun. 13 (2022), https://doi.org/10.1038/s41467-022-35664-w.

[25] Z.Y. Wu, M. Karamad, X. Yong, Q. Huang, D.A. Cullen, P. Zhu, C. Xia, Q. Xiao, M. Shakouri, F.Y. Chen, J.Y. (Timothy) Kim, Y. Xia, K. Heck, Y. Hu, M.S. Wong, Q. Li, I. Gates, S. Siahrostami, H. Wang, Electrochemical ammonia synthesis via nitrate reduction on Fe single atom catalyst, Nat. Commun. 12 (2021), https://doi.org/10.1038/s41467-021-23115-x.

[26] Y. Wang, C. Wang, M. Li, Y. Yu, B. Zhang, Nitrate electroreduction: mechanism insight, in situ characterization, performance evaluation, and challenges, Chem. Soc. Rev. 50 (2021) 6720–6733, https://doi.org/10.1039/d1cs00116g.

[27] Z. Guo, C. Ye, Y. Shen, Effects of electrolyte pHs, temperatures, potentials and oxalate ions on the electrocatalytic reduction of nitrates, J. Electroanal. Chem. 957 (2024), https://doi.org/10.1016/j.jelechem.2024.118143.

[28] Z. Wang, F. Zhou, B. Lv, J. Yu, J. Zhang, Y. Zhang, Y. Wu, Y. Wang, W. Luo, Unveiling pH-Dependent Mechanistic Shifts in Cu2O-Catalyzed Nitrate Electroreduction for Selective Ammonia Synthesis, Adv. Sustain. Syst. 9 (2025), https://doi.org/10.1002/adsu.202500211.

[29] Y. Xue, Q. Yu, Q. Ma, Y. Chen, C. Zhang, W. Teng, J. Fan, W.X. Zhang, Electrocatalytic Hydrogenation Boosts Reduction of Nitrate to Ammonia over Single-Atom Cu with Cu(I)-N3C1Sites, Environ. Sci. Technol. 56 (2022) 14797–14807, https://doi.org/10.1021/acs.est.2c04456.

[30] R.E. White, ed., Modern Aspects of Electrochemistry, 1st ed., Springer, New York, 209AD. https://doi.org/10.1007/978-1-4419-0655-7

[31] G.A. Kamat, J.A. Zamora Zeledón, G.T.K.K. Gunasooriya, S.M. Dull, J.T. Perryman, J.K. Nørskov, M.B. Stevens, T.F. Jaramillo, Acid anion electrolyte effects on platinum for oxygen and hydrogen electrocatalysis, Commun. Chem. 5 (2022), https://doi.org/10.1038/s42004-022-00635-1.

[32] M.T. Tang, J. Halldin Stenlid, J. Guo, E. Corson, W. Tarpeh, F. Abild-Pedersen, Nitrate Reduction Modeling under Acidic Conditions with Late Transition Metals, ACS Catal. 15 (2025) 4489–4498, https://doi.org/10.1021/acscatal.4c06394.

[33] J.X. Liu, D. Richards, N. Singh, B.R. Goldsmith, Activity and Selectivity Trends in Electrocatalytic Nitrate Reduction on Transition Metals, ACS Catal. 9 (2019) 7052–7064, https://doi.org/10.1021/acscatal.9b02179.

[34] M.R. Singh, Y. Kwon, Y. Lum, J.W. Ager, A.T. Bell, Hydrolysis of Electrolyte Cations Enhances the Electrochemical Reduction of CO2 over Ag and Cu, J. Am. Chem. Soc. 138 (2016) 13006–13012, https://doi.org/10.1021/jacs.6b07612.

[35] X. Chen, I.T. McCrum, K.A. Schwarz, M.J. Janik, M.T.M. Koper, Co-adsorption of Cations as the Cause of the Apparent pH Dependence of Hydrogen Adsorption on a Stepped Platinum Single-Crystal Electrode, Angew. Chem. 129 (2017) 15221–15225, https://doi.org/10.1002/ange.201709455.

[36] D. Strmcnik, K. Kodama, D. Van Der Vliet, J. Greeley, V.R. Stamenkovic, N. M. Marković, The role of non-covalent interactions in electrocatalytic fuel-cell reactions on platinum, Nat. Chem. 1 (2009) 466–472, https://doi.org/10.1038/nchem.330.

[37] A.N. Frumkin, Influence of cation adsorption on the kinetics of electrode processes, Trans. Faraday Soc. 55 (1959) 156–167, https://doi.org/10.1039/TF9595500156.

[38] M.C.O. Monteiro, A. Goyal, P. Moerland, M.T.M. Koper, Understanding Cation Trends for Hydrogen Evolution on Platinum and Gold Electrodes in Alkaline Media, ACS Catal. 11 (2021) 14328–14335, https://doi.org/10.1021/acscatal.1c04268.

[39] S. Qi, X. Chen, H. He, J. Wang, L. Li, Q. Huo, C. Shang, H. Yang, X. Zhang, Q. Hu, C. He, Unlocking the Critical Role of Noncovalent Interactions Between Alkali Metal Cations and Nitrate in Promoting the Reduction of Nitrate to Ammonia, Angew. Chem. Int. Ed. 64 (2025), https://doi.org/10.1002/anie.202520377.

[40] D. Zagorac, H. Muller, S. Ruehl, J. Zagorac, S. Rehme, Recent developments in the Inorganic Crystal Structure Database: Theoretical crystal structure data and related features, J. Appl. Crystallogr 52 (2019) 918–925, https://doi.org/10.1107/S160057671900997X.

[41] S. Graulis, D. Chateigner, R.T. Downs, A.F.T. Yokochi, M. Quirós, L. Lutterotti, E. Manakova, J. Butkus, P. Moeck, A. Le Bail, Crystallography Open Database - An open-access collection of crystal structures, J. Appl. Crystallogr 42 (2009) 726–729, https://doi.org/10.1107/S0021889809016690.

[42] N. Mahmood, Y. Yao, J.W. Zhang, L. Pan, X. Zhang, J.J. Zou, Electrocatalysts for Hydrogen Evolution in Alkaline Electrolytes: Mechanisms, Challenges, and Prospective Solutions, Adv. Sci. 5 (2017), https://doi.org/10.1002/advs.201700464.

[43] S. Trasatti, Work Function, Electronegativity, and Electrochemical Behaviour of Metals, J. Electroanal. Chem. Interfacial Electrochem 39 (1972) 163–184, https://doi.org/10.1016/S0022-0728(72)80485-6.

[44] Z.W. Seh, J. Kobsgaard, C.F. Dickens, I. Chorkendorff, J.K. Norskov, T.F. Jaramillo, Combining theory and experiment in electrocatalysis: Insights into materials design, Science 355 (1979) (2017), https://doi.org/10.1126/science.aad4998.

[45] E. Skúlason, V. Tripkovic, M.E. Björketun, S. Gudmundsdóttir, G. Karlberg, J. Rossmeisl, T. Bligaard, H. Jónsson, J.K. Nørskov, Modeling the electrochemical hydrogen oxidation and evolution reactions on the basis of density functional theory calculations, J. Phys. Chem. C. 114 (2010) 18182–18197, https://doi.org/10.1021/jp1048887.

[46] C.M. Mendez, H. Olivero, D.E. Damiani, M.A. Volpe, On the role of Pd β-hydride in the reduction of nitrate over Pd based catalyst, Appl. Catal. B 84 (2008) 156–161, https://doi.org/10.1016/j.apcatb.2008.03.019.

[47] B. Wickman, M. Fredriksson, L. Feng, N. Lindahl, J. Hagberg, C. Langhammer, Depth probing of the hydride formation process in thin Pd films by combined electrochemistry and fiber optics-based in situ UV/vis spectroscopy, Phys. Chem. Chem. Phys. 17 (2015) 18953–18960, https://doi.org/10.1039/c5cp01339a.

[48] J. Wen, Z. Wan, X. Hu, J. Huang, X. Kang, Restructuring of copper catalysts by potential cycling and enhanced two-carbon production for electroreduction of carbon dioxide, J. CO2 Util. 56 (2022), https://doi.org/10.1016/j.jcou.2021.101846.

[49] N. Kachi, G. Verma, A. Suzuki, G. Jerkiewicz, A. Kuzume, Influence of Surface Oxides on the Electrochemical Behaviour of Ni(111) in the Hydrogen Evolution Potential Region, Electrocatalysis (2026), https://doi.org/10.1007/s12678-026-01030-3.

[50] J. Fan, Z. Feng, Y. Mu, X. Ge, D. Wang, L. Zhang, X. Zhao, W. Zhang, D.J. Singh, J. Ma, L. Zheng, W. Zheng, X. Cui, Spatially Confined PdHx Metallenes by Tensile Strained Atomic Ru Layers for Efficient Hydrogen Evolution, J. Am. Chem. Soc. 145 (2023) 5710–5717, https://doi.org/10.1021/jacs.2c11692.

[51] A.C.A. De Vooys, M.T.M. Koper, R.A. Van Santen, J.A.R. Van Veen, Mechanistic study on the electrocatalytic reduction of nitric oxide on transition-metal electrodes, J. Catal. 202 (2001) 387–394, https://doi.org/10.1006/jcat.2001.3275.

[52] J. Zheng, T. Lu, T.M. Cotton, G. Chumanov, Photoinduced Electrochemical Reduction of Nitrite at an Electrochemically Roughened Silver Surface, J. Phys. Chem. B 103 (1999) 6567–6572, https://doi.org/10.1021/jp990928h.

[53] M. Duca, M.C. Figueiredo, V. Climent, P. Rodriguez, J.M. Feliu, M.T.M. Koper, Selective Catalytic Reduction at Quasi-Perfect Pt (100) Domains: A Universal Low-Temperature Pathway from Nitrite to N2, J. Am. Chem. Soc. 133 (2011) 10928–10939, https://doi.org/10.1021/ja203234v.

[54] M.M. Waegele, C.M. Gunathunge, J. Li, X. Li, How cations affect the electric double layer and the rates and selectivity of electrocatalytic processes, J. Chem. Phys. 151 (2019), https://doi.org/10.1063/1.5124878.

[55] F. Domínguez-Flores, A. Groß, W. Schmickler, Cation-Induced Dipole Moments on Single-Crystal Metal Surfaces, J. Phys. Chem. C. 129 (2025) 9179–9188, https://doi.org/10.1021/acs.jpcc.5c01062.

[56] J.N. Mills, I.T. McCrum, M.J. Janik, Alkali cation specific adsorption onto fcc(111) transition metal electrodes, Phys. Chem. Chem. Phys. 16 (2014) 13699–13707, https://doi.org/10.1039/c4cp00760c.

[57] J.W. Schultze, D. Rolle, The partial discharge of electrosorbates and its influence in electrocatalysis, Can. J. Chem. 75 (1997) 1750–1758, https://doi.org/10.1139/v97-608.

[58] J. Mähler, I. Persson, A study of the hydration of the alkali metal ions in aqueous solution, Inorg. Chem. 51 (2012) 425–438, https://doi.org/10.1021/ic2018693.

[59] I. Persson, Hydrated metal ions in aqueous solution: how regular are their structures? Pure Appl. Chem. (2010) 1901–1917, https://doi.org/10.1351/PAC-CON-09-10-22.

[60] A.S. Fajardo, P. Westerhoff, S. Garcia-Segura, C.M. Sánchez-Sánchez, Selectivity modulation during electrochemical reduction of nitrate by electrolyte engineering, Sep. Purif. Technol. 321 (2023), https://doi.org/10.1016/j.seppur.2023.124233.

[61] J.T. Bender, A.S. Petersen, F.C. Østergaard, M.A. Wood, S.M.J. Heffernan, D. J. Milliron, J. Rossmeisl, J. Resasco, Understanding cation effects on the hydrogen evolution reaction, ACS Energy Lett. 8 (2023) 657–665, https://doi.org/10.1021/acsenergylett.2c02500.